doi:10.1093/jmcb/mjaa081
Published online January 20, 2021

Article

Ablation of *Zfhx4* results in early postnatal lethality by disrupting the respiratory center in mice

Meiqin Zhang[1,†], Sichen Du[1,†], Huayuan Ou[1], Renjie Cui[1], Nan Jiang[1], Yifeng Lin[2], Runsheng Ge[1], Duan Ma[1,2,*], and Jin Zhang[1,*]

[1] Key Laboratory of Metabolism and Molecular Medicine, Ministry of Education, Department of Biochemistry and Molecular Biology, School of Basic Medical Sciences & Institutes of Biomedical Sciences, Shanghai Medical College, Fudan University, Shanghai 200032, China
[2] Children's Hospital, Fudan University, Shanghai 201102, China
[†] These authors contributed equally to this work.
[*] Correspondence to: Duan Ma, E-mail: duanma@fudan.edu.cn; Jin Zhang, E-mail: jinzhang@fudan.edu.cn

Edited by Zhen-Ge Luo

Breathing is an integrated motor behavior that is driven and controlled by a network of brainstem neurons. Zfhx4 is a zinc finger transcription factor and our results showed that it was specifically expressed in several regions of the mouse brainstem. Mice lacking Zfhx4 died shortly after birth from an apparent inability to initiate respiration. We also found that the electrical rhythm of brainstem–spinal cord preparations was significantly depressed in *Zfhx4*-null mice compared to wild-type mice. Immunofluorescence staining revealed that Zfhx4 was coexpressed with Phox2b and Math1 in the brainstem and that Zfhx4 ablation greatly decreased the expression of these proteins, especially in the retrotrapezoid nucleus. Combined ChIP–seq and mRNA expression microarray analysis identified *Phox2b* as the direct downstream target gene of Zfhx4, and this finding was validated by ChIP–qPCR. Previous studies have reported that both Phox2b and Math1 play key roles in the development of the respiratory center, and *Phox2b* and *Math1* knockout mice are neonatal lethal due to severe central apnea. On top of this, our study revealed that Zfhx4 is a critical regulator of Phox2b expression and essential for perinatal breathing.

Keywords: parafacial respiratory group, Phox2b, respiratory center, Zfhx4

Introduction

Breathing is an integrated motor behavior that is driven and controlled by a network of brainstem neurons that are distributed in several brainstem respiratory compartments from the rostral pons to the caudal medulla, especially the pontine respiratory group (PRG) in the pons, and the ventral respiratory group (VRG) and the dorsal respiratory group (DRG) in the medulla. It is believed that the DRG and VRG are essential for basic respiration generation, while the PRG only exerts fine control over medullary neurons (Champagnat et al., 2011). Respiratory rhythm in mammals is generated by a close collaboration between the pre-Bot-zinger complex (preBotc) and the parafacial respiratory group (pFRG) neurons within the VRG of the medulla (Lieske et al., 2000; Onimaru and Homma, 2003; Blanchi and Sieweke, 2005). The preBotc generates inspiratory breathing rhythms, and the pFRG has been proposed to function as a preinspiratory or expiratory-modulating nucleus in newborns (Rose et al., 2009). Additionally, the retrotrapezoid nucleus (RTN), which is part of the VRG of the medulla, contains CO_2-sensitive neurons around the ventral and medial edges of the facial nucleus, controls respiratory responses to changes in blood pH, and affects both inspiratory and expiratory activities (Onimaru et al., 2012; Keiko et al., 2016; Pisanski and Pagliardini, 2019). The pFRG at least partially overlaps with the RTN, and the debate concerning whether the pFRG and the RTN are anatomically and functionally distinct is ongoing. In recent years, accumulating evidence supports that RTN and pFRG are

Received March 10, 2020. Revised November 19, 2020. Accepted December 7, 2020.

two functionally distinct populations of neurons (Zoccal et al., 2018; Pisanski and Pagliardini, 2019).

Through the analysis of mouse mutants with central breathing defects, some genes specifying the development and identity of critical rhythm-generating neurons in the brainstem have been identified, such as paired-like homeobox 2b (*Phox2b*) (Dubreuil et al., 2008; Goridis et al., 2010), ladybird homeobox homolog 1 (*Lbx1*) (Pagliardini et al., 2008), atonal basic helix loop helix transcription factor 1 *(Atoh1*, also known as *Math1*) (Machold and Fishell, 2009; Rose et al., 2009), the hindbrain segmentation gene Egr2 (*Krox20*) (Thoby-Brisson et al., 2009; Ray et al., 2013), and *MafB* (Blanchi et al., 2003). In the hindbrain, *Lbx1* and *Phox2b* are coexpressed in a population of dB2 neurons and contribute to proper dB2 neuron development (Pagliardini et al., 2008; Hernandez-Miranda et al., 2018). In the VRG, *Math1* is exclusively expressed in dB2 neurons of the RTN (Ruffault et al., 2015; Hernandez-Miranda et al., 2017). All mice with mutations in *Phox2b*, *Lbx1*, or *Math1* show disruption of the RTN and respiratory rhythm impairment and die immediately or shortly after birth from an apparent inability to initiate respiration (Ben-Arie et al., 1997; Dubreuil et al., 2008; Pagliardini et al., 2008; Machold and Fishell, 2009; Rose et al., 2009).

Some human disorders involve defects in the central control of breathing, such as central hypoventilation syndrome (CCHS) (Ramanantsoa and Gallego, 2013), central sleep apnea syndrome (Wuyam et al., 2000; Yap and Fleetham, 2001), and some cases of sudden infant death syndrome (Calton et al., 2016; Porzionato et al., 2018). CCHS, which is often present at birth, is a genetic disease in which the brain fails to properly control breathing to maintain healthy levels of oxygen and carbon dioxide, especially during sleep, and a mutation in PHOX2B is the only confirmed heterozygous mutation causing CCHS (Amiel et al., 2003; Trochet et al., 2005; Weese-Mayer et al., 2017). To date, the physiological and molecular basis and potential genetic susceptibilities underlying most cases of central respiratory disorders remain elusive.

Proteins of zinc finger homeobox (ZFHX) family are transcription factors containing zinc finger motifs and homeodomains. Four ZFHX proteins have been identified in vertebrates, including Zfhx1, Zfhx2, Zfhx3, and Zfhx4. Among them, Zfhx4 has ~3550 amino acids and carries four homeodomains and 22 zinc fingers including two pseudo zinc finger motifs (Hemmi et al., 2006). *Zfhx4* is prominently expressed in developing brains and muscles, and its expression is highest in the embryonic period and gradually decreases to barely detectable levels in adulthood. *Zfhx4* is induced to be expressed during neuronal differentiation in postnatal day 19 (P19) embryonal carcinoma cells (Kostich and Sanes, 1995; Sakata et al., 2000; Hemmi et al., 2006). *ZFHX4* was identified as a candidate gene for congenital ptosis, which is defined as drooping of the upper eyelid (McMullan et al., 2002; Nakashima et al., 2008). Furthermore, *ZFHX4* is the only protein-coding gene in the minimum deletion region of 8q21.11 microdeletion syndrome, the clinical symptoms of which consist of intellectual disability, decreased balance, sensorineural hearing loss, unusual behavior, and some facial characteristics (Palomares et al., 2011). A Previous study also revealed that *ZFHX4* was required to maintain glioblastoma tumor-initiating cell-associated and normal human neural precursor cell phenotypes (Chudnovsky et al., 2014). In this research, we found that *Zfhx4* was specifically expressed in several regions of the hindbrain and its ablation causes defective respiratory rhythmogenesis.

Results

Zfhx4 expression is enriched in the brainstem

To evaluate tissue distribution, *Zfhx4* mRNA expression was measured by using quantitative reverse-transcription polymerase chain reaction (qRT-PCR) of heart, liver, spleen, lung, kidney, stomach, cerebral cortex, and brainstem tissues from early postnatal mice (P0), and the results showed that *Zfhx4* transcripts were highly expressed in the brainstem (Figure 1A). *Zfhx4* mRNA was also detected in the brainstem on embryonic day 12.5 (E12.5), E16.5, P0, P5, and P10 during brain development; the expression of *Zfhx4* was highest on E16.5 and gradually decreased postnatally (Figure 1B). Polyclonal antibodies against Zfhx4 were generated by immunizing rabbits with the recombinant glutathione S-transferase (GST)-Zfhx4 (amino acid residues 2677–2884) fusion protein and affinity purification with immobilized antigen. The purified anti-Zfhx4 antibody was used to detect Zfhx4 protein expression in the E16.5 mouse brain by using immunofluorescence staining. As shown in Figure 1C, the Zfhx4 protein was expressed in the midbrain and hindbrain, with several clusters of Zfhx4-positive cells near the PRG, VRG, and DRG. The Zfhx4 protein was localized in the cell nucleus, and double immunofluorescence staining showed that the Zfhx4 protein was mainly expressed in NeuN-positive neurons (Figure 1D).

Zfhx4-deficient mice are generated by insertion of the PB transposon

PiggyBac (*PB*) is a DNA transposon, and its insertion can ablate gene expression to facilitate the identification of gene function, making it a useful genetic manipulation tool in mice (Ding et al., 2005; Li et al., 2016; Friedrich et al., 2019; Weber et al., 2019). To explore the biological function of *Zfhx4*, we used a H362cR1 *PB* insertion mouse line, in which a modified *PB* transposon element was inserted into the third intron of the *Zfhx4* gene (Campbell et al., 2002; Ding et al., 2005; Sun et al., 2008). The inserted transposon element contains the DNA sequence of β-actin promoter-monomeric red fluorescent protein (*Act*-mRFP) flanked by *PB*-specific left and right terminal sequences (PBL and PBR, respectively), and the insertion site of *PB* transposon element was confirmed by DNA sequencing (Figure 2A). The genotype of each mouse was determined by PCR amplification of genomic DNA. A 350-bp PCR product was amplified from the wild-type (WT) allele, and a 250-bp product was amplified from

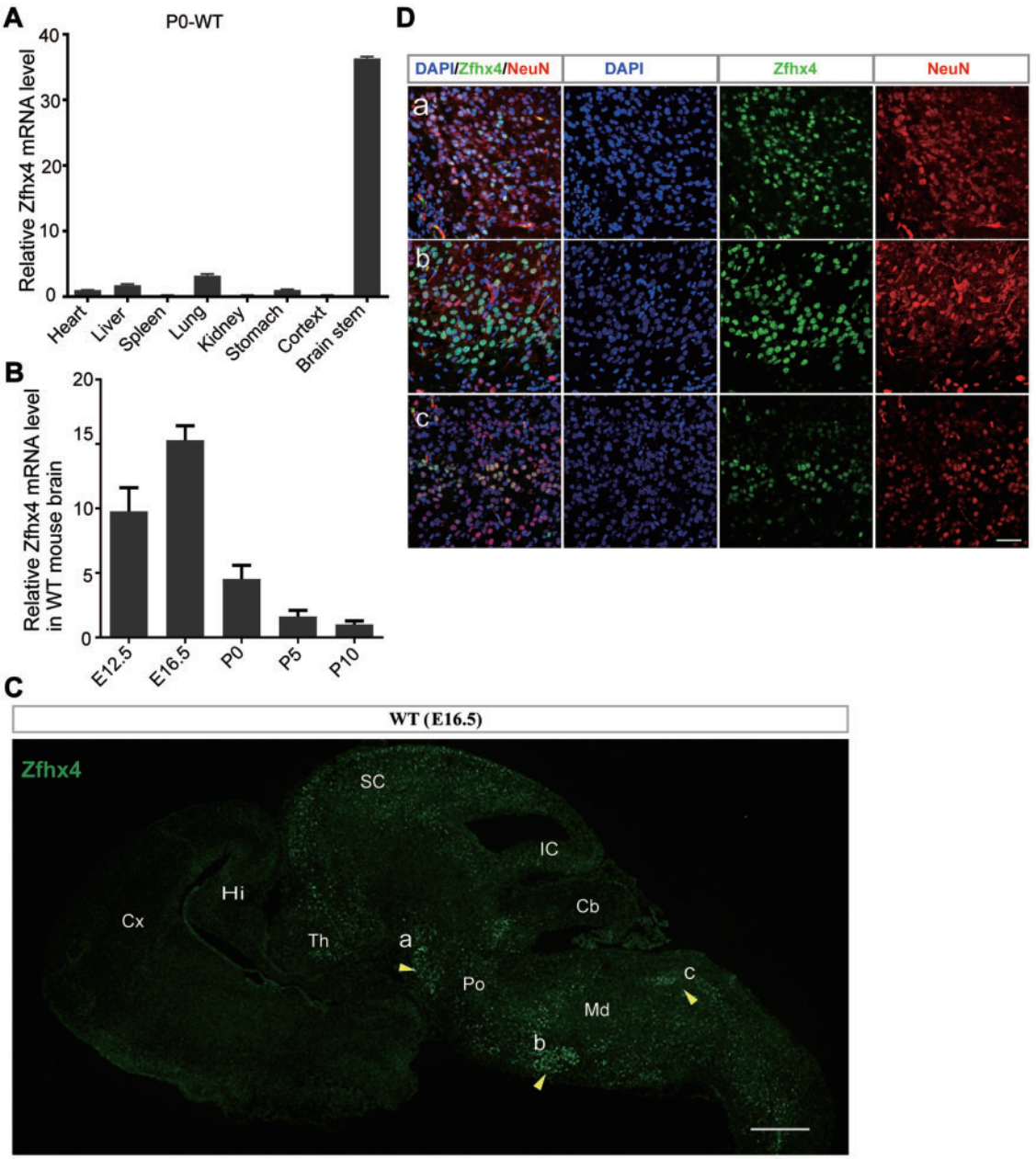

Figure 1 Distribution of Zfhx4 in mouse brain. (**A**) Real-time PCR results showing that *Zfhx4* was highly expressed in the brainstem compared to other organs in P0 mice. Data are expressed as mean ± SD, $n = 3$. (**B**) qRT-PCR analysis of *Zfhx4* expression in the mouse brainstems at different ages, revealing that *Zfhx4* mRNA had the highest expression in the E16.5 mouse brains and decreased after birth. Data are expressed as mean ± SD, $n = 3$. (**C**) Immunofluorescence staining of E16.5 WT mouse brain. Zfhx4 was mainly expressed in the brainstem. Immunoreactive signals were detected in thalamus (Th), superior colliculus (SC), pons (Po), and medulla (Md) but not detectable in cerebral cortex (Cx) and hippocampus (Hi). (**D**) Magnified views of the selected regions (indicated by yellow arrowheads) in **C**, showing Zfhx4 (green) colocated with DAPI (blue) and mainly expressed in NeuN-labelled neurons (red). Scale bar, 500 μm (**C**) and 200 μm (**D**).

the *PB*-inserted allele (Figure 2B). Results from qRT-PCR showed that *Zfhx4* mRNA was decreased in the brainstems of *Zfhx4*$^{PB/+}$ mice compared to those of WT mice and was almost completely undetectable in *Zfhx4*$^{PB/PB}$ mice (Figure 2C). Furthermore, both western blotting and immunofluorescence staining results demonstrated that the Zfhx4 protein was almost undetectable in the brainstems of *Zfhx4*$^{PB/PB}$ mice (Figure 2D–F). Taken together, these data suggested that the *Zfhx4* gene was effectively ablated in *Zfhx4*$^{PB/PB}$ mice. Furthermore, after the sections were fixed and stained for

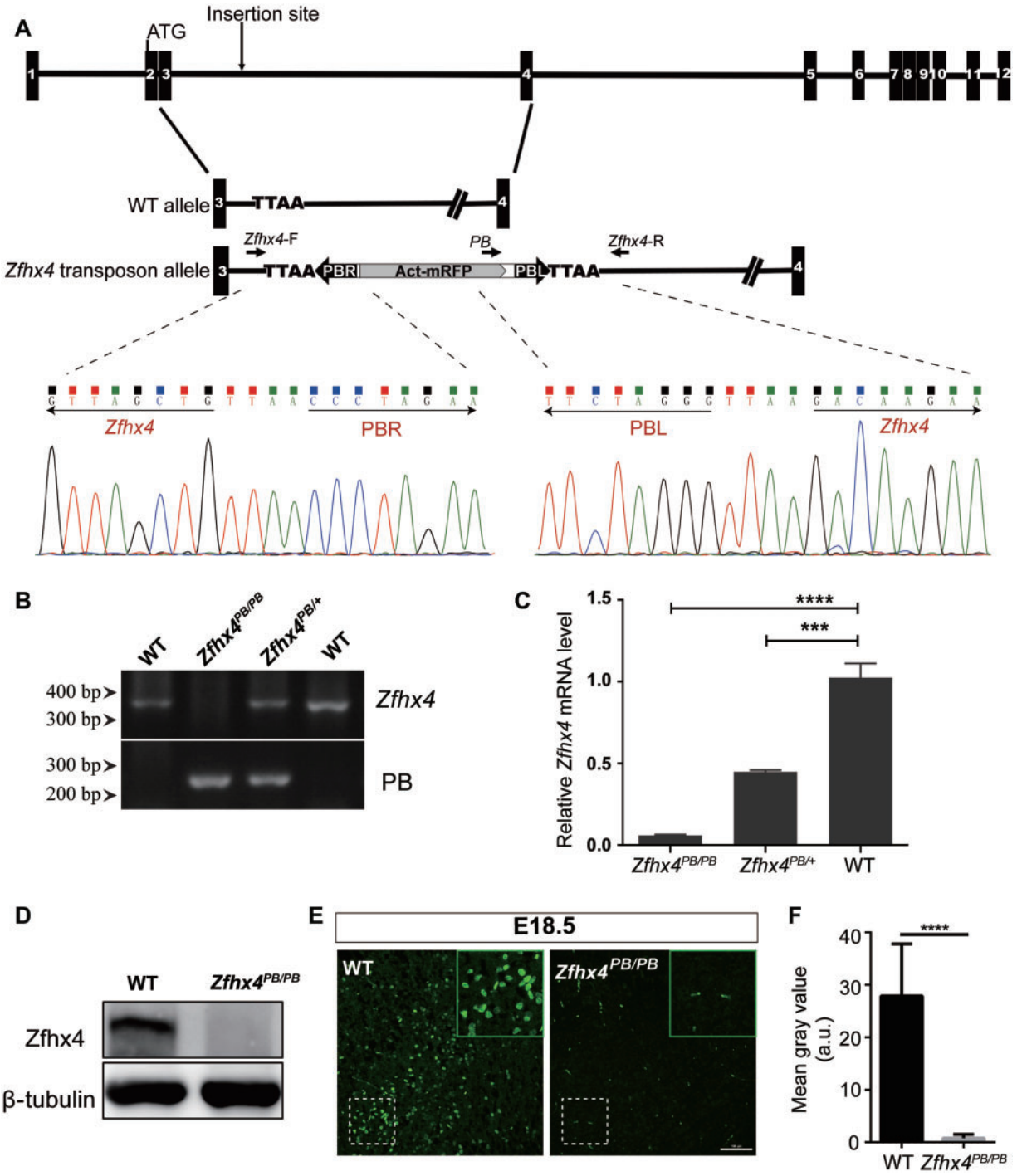

Figure 2 *Zfhx4*-deficient mice are generated by insertion of the *PB* transposon. (**A**) Diagram of *PB* transposon insertion site in the mouse *Zfhx4* gene. The *PB* transposon element contains the DNA fragment of *Act*-mRFP flanked by PB-specific left and right terminal sequences PBL and PBR (black arrows). In $Zfhx4^{PB/PB}$ mice, the *PB* transposon was integrated to the third intron of the *Zfhx4* gene. The WT allele or *PB*-inserted allele of *Zfhx4* was measured by using the Zfhx4-F primer or the PB primer with the common reverse Zfhx4-R primer. The insertion site of *PB* transposon was amplified and confirmed by DNA sequencing. (**B**) PCR-based genotyping of homozygous $Zfhx4^{PB/PB}$ (281 bp), heterozygous $Zfhx4^{PB/+}$ (346 and 281 bp), and WT (346 bp) mice. (**C** and **D**) qRT-PCR (**C**) and western blotting (**D**) analyses showing that the expression of *Zfhx4* was almost completely knocked down in the $Zfhx4^{PB/PB}$ mice. Data are expressed as mean ± SD. $^{**}P < 0.001$, $^{****}P < 0.0001$ (one-way ANOVA), $n = 3$. (**E** and **F**) Representative immunofluorescence images (**E**) and quantification for the mean gray values (**F**) of Zfhx4 in E18.5 $Zfhx4^{PB/PB}$ and WT mouse brains (region c in Figure 1C), showing that Zfhx4 (green) was lost in the $Zfhx4^{PB/PB}$ mouse brains. Scale bar, 100 μm. a.u., arbitrary units. Data are expressed as mean ± SD. $^{****}P < 0.0001$ (Student's *t*-test), $n = 15$.

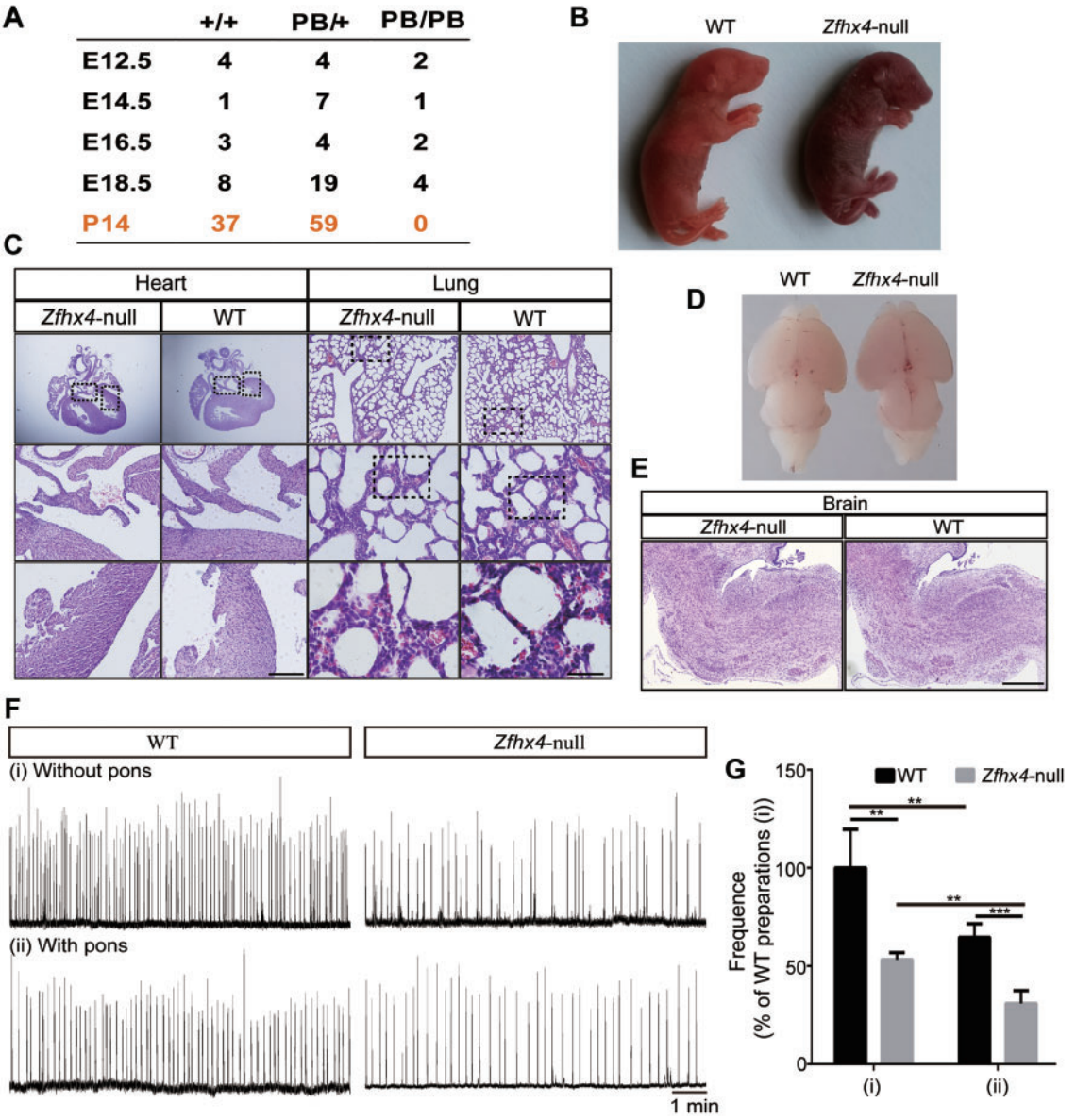

Figure 3 *Zfhx4*-null mice die within 24 h after birth and display slow central respiratory rhythm. (**A**) The number of embryos at the indicated stages of development and the number of neonates at P14. (**B**) A representative image showing that newborn *Zfhx4*-null mice became cyanotic compared with the WT mice. (**C**) Pathologic analysis showed no evident lesions in heart and lung tissues of neonatal *Zfhx4*-null mice compared with the WT mice. Scale bar, 200 μm. (**D**) A representative image showing no difference in brain size between WT and *Zfhx4*-null newborn mice. (**E**) Pathologic analysis showing no evident lesions in brains of neonatal *Zfhx4*-null mice compared with the WT mice. Scale bar, 200 μm. (**F**) Rectified and integrated suction electrode recordings obtained from the brainstem–spinal cord preparations. Respiratory output recorded from the C4 ventral root of preparations containing or lacking the pons from P0 WT mice (left column) and *Zfhx4*-null mice (right column) under normoxic condition. (**G**) Population data of respiratory frequency from WT (black) and *Zfhx4*-null (gray) mice for each brainstem–spinal cord preparation (i and ii) depicted in **F**. Data were normalized to that of WT preparation (i) for ease of comparison. Data are expressed as mean ± SD. $^{**}P < 0.01$, $^{***}P < 0.001$ (Student's *t*-test). (i) WT, $n = 7$; *Zfhx4*-null, $n = 3$; (ii) WT, $n = 5$; *Zfhx4*-null, $n = 4$.

immunofluorescence, the mRFP became invisible in frozen $Zfhx4^{PB/PB}$ brain tissue sections and did not interfere with the signal of the red fluorescent dye Alexa Fluor 594 used in our subsequent studies (Supplementary Figure S1).

Phenotypic analysis of Zfhx4-null mice

Heterozygous $Zfhx4^{PB/+}$ mice were fertile and showed no grossly apparent phenotype compared to WT controls. Following intercrossing of heterozygous mice, the genotypes of

the progeny were determined 2–3 weeks after birth, and no homozygous *Zfhx4*$^{PB/PB}$ mice were identified. Genotype analysis from E12.5 to E18.5 showed that *Zfhx4*$^{PB/PB}$ mice were born at the expected Mendelian ratio (Figure 3A). Close observation of pregnant mice at delivery showed that *Zfhx4*-null pups were born normally but exhibited gasping behavior and cyanosis and died within the first 24 h after birth (Figure 3B; Supplementary Movie). No anatomical or histological abnormalities in the hearts and lungs of neonatal *Zfhx4*-null mice were identified by hematoxylin and eosin (H&E) staining (Figure 3C). Furthermore, there were no obvious morphological or structural abnormalities in the whole brains or brainstems of neonatal *Zfhx4*-null mice (Figure 3D and E). Considering the gasping behavior and cyanosis observed in neonatal *Zfhx4*-null mice and the high expression of *Zfhx4* specifically in the brainstem, we speculated that these mice suffered from central neurogenic respiratory failure. Electrical activity corresponding to phrenic nerve activity was monitored from the fourth cervical ventral root (C4) of *in vitro* brainstem–spinal cord preparations from neonatal (P0) mice, and two types of hindbrain models were measured, including (i) medulla (standard preparation) and (ii) cerebellum–pons–medulla (Figure 3F). Previous studies have shown that the pons, located in the rostral part of the brainstem, has an inhibitory action on the rhythm generator and inspiratory burst amplitude (Okada, 1998; Caravagna et al., 2014), and our results also showed that respiratory frequency was significantly decreased in the cerebellum–pons–medulla preparation compared with the medulla preparation. The respiratory frequencies of both *Zfhx4*-null hindbrain preparations (i and ii, right columns) were significantly decreased compared with that of the corresponding WT hindbrain preparations (Figure 3G), which indicates that *Zfhx4*-null mice have abnormal respiration and the defective respiratory rhythmogenesis lies within the medulla.

Abnormal gene expression profile of the Zfhx4-null brainstem

Zfhx4 was expressed in several regions of the brainstem in WT mice, but no obvious morphologic abnormalities were observed in these areas of *Zfhx4*-null mice. To identify the key function and mechanism of *Zfhx4* in the establishment of normal newborn breathing, the gene expression profile of P0 *Zfhx4*-null brainstem was detected by using microarrays. The microarrays contained probes for 33075 mouse genes. Analysis of the normalized data revealed a list of differentially expressed genes (with fold change ≥ 2 or ≤ 0.5, q-value ≤ 0.05), among which 324 genes were differentially expressed between *Zfhx4*-null and WT mice, including 37 upregulated genes and 287 downregulated genes (Supplementary Table S1). Hierarchical clustering of the differentially expressed genes showed a clear distinction between WT and *Zfhx4*-null mouse brainstems (Figure 4A). Gene ontology (GO) enrichment analysis of the differentially expressed genes revealed that several nervous system development-associated processes are modulated by *Zfhx4*, such as neural generation and differentiation (Figure 4B). Several respiratory center development-associated genes were found to be decreased in *Zfhx4*-null mice (Figure 4C), among which *Phox2b*, *Math1*, and *Lbx1* have been reported to play key roles in the development of the respiratory center. Furthermore, *Phox2b*, *Math1*, and *Lbx1* knockout mice also die at birth due to severe central apnea, which is consistent with the phenotype of *Zfhx4*-null mice (Dubreuil et al., 2008; Pagliardini et al., 2008; Machold and Fishell, 2009; Rose et al., 2009; Goridis et al., 2010). The expression levels of *Math1*, *Phox2b*, and *Lbx1*, along with some other identified nerve development-associated genes, were further validated in another group of brainstem samples by using qPCR (Figure 4D).

Phox2b and Math1 are coexpressed with Zfhx4 in the brainstem and their expression levels are reduced in Zfhx4-null mice

Immunofluorescence staining showed that the Zfhx4 protein was coexpressed with Phox2b in several regions of the P0 mouse brainstem, including the locus coeruleus (LC), facial motor (VII), rostral nucleus of the solitary tract (rNTS), and DRG, while the expression of Phox2b was greatly decreased in *Zfhx4*-null mice compared to WT mice (Figure 5, B′ vs. B″, C′ vs. C″, D′ vs. D″, E′ vs. E″). Additionally, because a non-rabbit anti-Math1 antibody is not available, Math1-Cre mice were used to assess Math1 expression by anti-Cre staining. In P0 Math-Cre mice, Zfhx4 was coexpressed with Math1-Cre in the cerebellum and paratrigeminal region (around the trigeminal motor, V) (Figure 6A–H; Rose et al., 2009). Math1 expression and the number of Math1-positive cells were decreased in *Zfhx4*-null mice compared to WT mice (Figure 6I–J″). Moreover, the expression of Lbx1 was also greatly reduced in the cerebellum, medial vestibular nucleus, parvicellular part (MvePC), paratrigeminal region, and preBotc in *Zfhx4*-null mice compared to WT mice (Supplementary Figure S2).

Ablation of Zfhx4 leads to abnormal development of RTN neurons

The RTN is composed of a small population of heterogeneous neurons surrounding the facial motor nucleus (VIIn) of the ventrolateral medulla that coexpress Phox2b, Lbx1, and Math1 (Pagliardini et al., 2008; Rose et al., 2009; Ruffault et al., 2015; Hernandez-Miranda et al., 2017, 2018). Previous studies have shown that deletion of *Math1*, *Phox2b*, or *Lbx1* led to abnormal development of the RTN (Dubreuil et al., 2008; Pagliardini et al., 2008; Machold and Fishell, 2009; Rose et al., 2009; Goridis et al., 2010). Thus, we further evaluated RTN neurons in *Zfhx4*-null mice. At P0, Zfhx4-positive neurons that were Phox2b^{+}/Math1^{+} or Phox2b^{+}/Lbx1^{+} appeared in the RTN region (Figure 7B and C), and Zfhx4 coexpressed with Phox2b in the RTN (Figure 7A and D). The expression levels of Phox2b, Math1, and Lbx1 were greatly decreased in the RTN in P0 *Zfhx4*-null

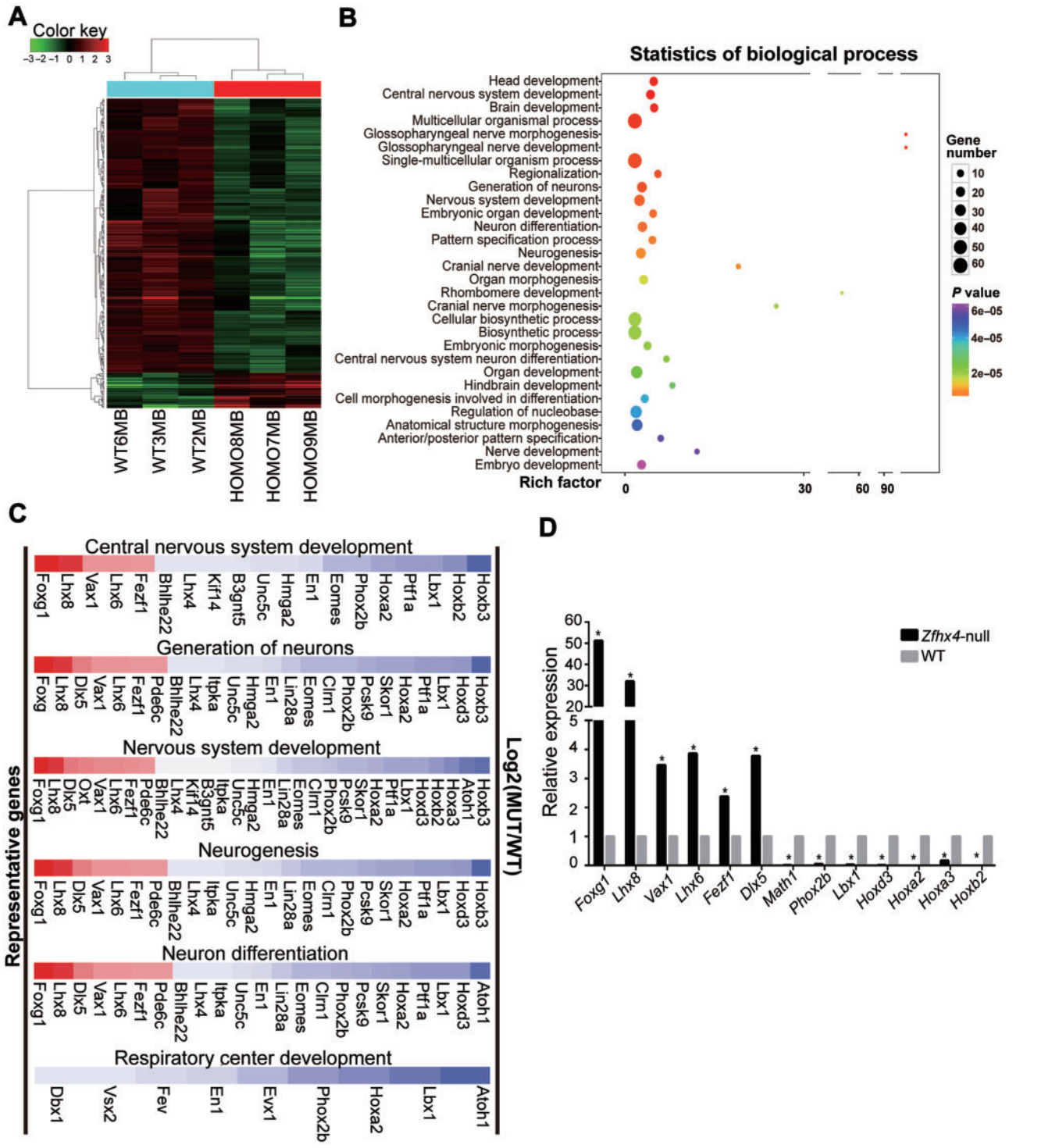

Figure 4 Microarray and bioinformatics analysis of gene expression in *Zfhx4*-null mouse brainstems. (**A**) Expression microarray was performed using RNA isolated from WT and *Zfhx4*-null mouse brainstems on P0. The heat map of the gene expression microarray shows the striking difference in overall gene expression between *Zfhx4*-null and WT mice. Green and red indicate decreased and increased signal intensity/expression compared to the median signal intensity across all samples, respectively. (**B**) GO analysis of the differentially expressed genes in *Zfhx4*-null mouse brainstems, showing that many differentially expressed genes were enriched in nervous system development, including hindbrain development ($P < 0.001$). (**C**) Representative genes related to nervous development shown by log2(MUT/WT) of expression changes. Red and blue colors represent upregulated and downregulated genes, respectively. MUT, mutant. (**D**) The selected genes were further validated by qRT-PCR. Data are presented as mean ± SD. *$P < 0.05$ (Student's *t*-test), $n = 3$.

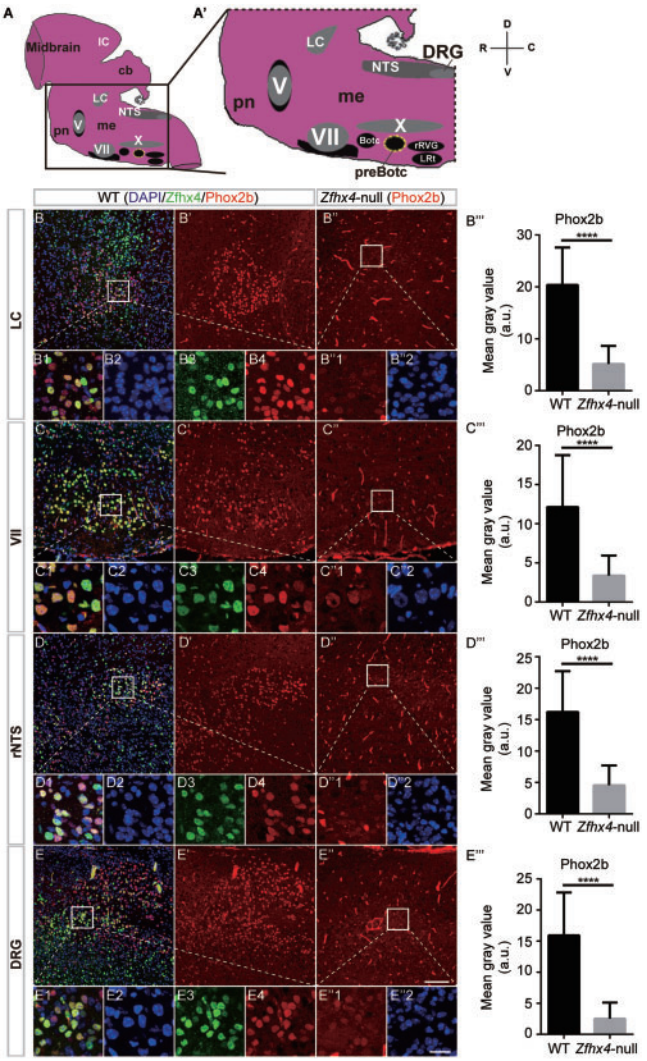

Figure 5 Phox2b is coexpressed with Zfhx4 in brainstem and its expression levels are reduced in *Zfhx4*-null mice. (**A** and **A**′) Sagittal model of the hindbrain, with midbrain at top, showing the motor nuclei V, VII, and X (all gray), the ventral respiratory nuclei (black), and NTS/DRG (gray) in the medulla. V, trigeminal motor; VII, facial motor; X, ambiguous. (**B**–**E**‴) Immunofluorescent staining for Zfhx4 (green) and Phox2b (red) in LC, VII, rNTS, and DRG from P0 WT and *Zfhx4*-null mouse brainstems and quantification for the mean gray values of red immunofluorescence. DAPI was used to stain nuclei. Insets are magnified views of the selected regions indicated by solid white rectangles. Phox2b displayed colocalization with Zfhx4 in nucleus in the LC, VII, rNTS, and DRG of P0 WT mice but greatly decreased expression in these regions of P0 *Zfhx4*-null mice. Scale bar, 100 μm and 25 μm (insets). Data in bar graphs are expressed as mean ± SD. ****$P < 0.0001$ (Student's *t*-test), $n = 15$.

mice compared to P0 WT mice (Figure 7E–G). As described by Czeisler et al. (2019), a subset of RTN astrocytes derive from Phox2b$^+$ precursors. Therefore, we also used immunofluorescence staining to determine whether Zfhx4 is expressed in GFAP-positive astrocytes in the mouse brain. The results showed that both GFAP and Zfhx4 were expressed in the ventral margin of the medulla but not colocalized (Supplementary Figure S3). Furthermore, the RTN is the main determinant of the CO_2/H^+-dependent drive to breathe (Dubreuil et al., 2009; Goridis et al., 2010; Fu et al., 2017). Compared with medulla–spinal cord preparations from WT mice, *Zfhx4*-null medulla–spinal cord preparations failed to increase respiratory output in response to acidification (Supplementary Figure S4). These results showed that *Zfhx4* was essential for the development of the RTN.

Phox2b is the direct downstream target gene of Zfhx4

Zfhx4 is a multi-zinc finger transcriptional factor located in the nucleus. To identify genes that are transcriptionally regulated directly by Zfhx4, chromatin immunoprecipitation coupled with high-throughput sequencing (ChIP–seq) was used to isolate the Zfhx4-binding DNA fragments in mouse brainstem tissues on E16.5. Using $P < 0.005$ as the threshold for significance, a total of 1795 peaks were detected in the Zfhx4 ChIP–seq data set and 1410 known genes were identified to be associated with these peaks (Supplementary Table S2). GO enrichment analysis of genes associated with Zfhx4 peaks identified a number of processes involved in neuronal development, including neuronal differentiation and neurogenesis (Figure 8A). Integrating the ChIP–seq data with gene expression microarray data, 46 genes were found to overlap (Figure 8B). Among the 46 genes, the DNA fragment of 994 bp (chr5:67098188–67098426) downstream from the transcription initiation site of the *Phox2b* gene was identified to be bound by Zfhx4 (Figure 8C). The binding of Zfhx4 to the downstream region of the *Phox2b* promoter was further validated by ChIP–qPCR (Figure 8D).

The above results showed that the mRNA and protein expression of *Zfhx4* was greatly decreased in the *Zfhx4*-null brainstem compared to WT brainstem and Phox2b was coexpressed with Zfhx4 in several regions of the brainstem. The embryonic parafacial oscillator (ePF), presumably the embryonic equivalent to the pFRG, is formed by a small population of Phox2b-expressing neurons near the facial nucleus on E14.5 in mice (Feldman et al., 2013). We next measured the expression of Zfhx4 and Phox2b during the early development of ePF. In the E10.5 and E12.5 hindbrain, Zfhx4 was expressed mainly on the ventral side and showed a similar expression distribution and colocalization as Phox2b (Figure 8E, a and b). On E14.5, Zfhx4$^+$/Phox2b$^+$ neurons were mainly located in the facial nucleus and ambiguous region (X), and Zfhx4 was also coexpressed with Phox2b in the newly formed ePF (Figure 8E, c). We also observed colocalization of Zfhx4 and Phox2b in the early embryonic paratrigeminal arrangements (Figure 8E, d–f).

Discussion

Central control of breathing occurs in the brainstem, which contains neurons that directly generate respiratory rhythms or

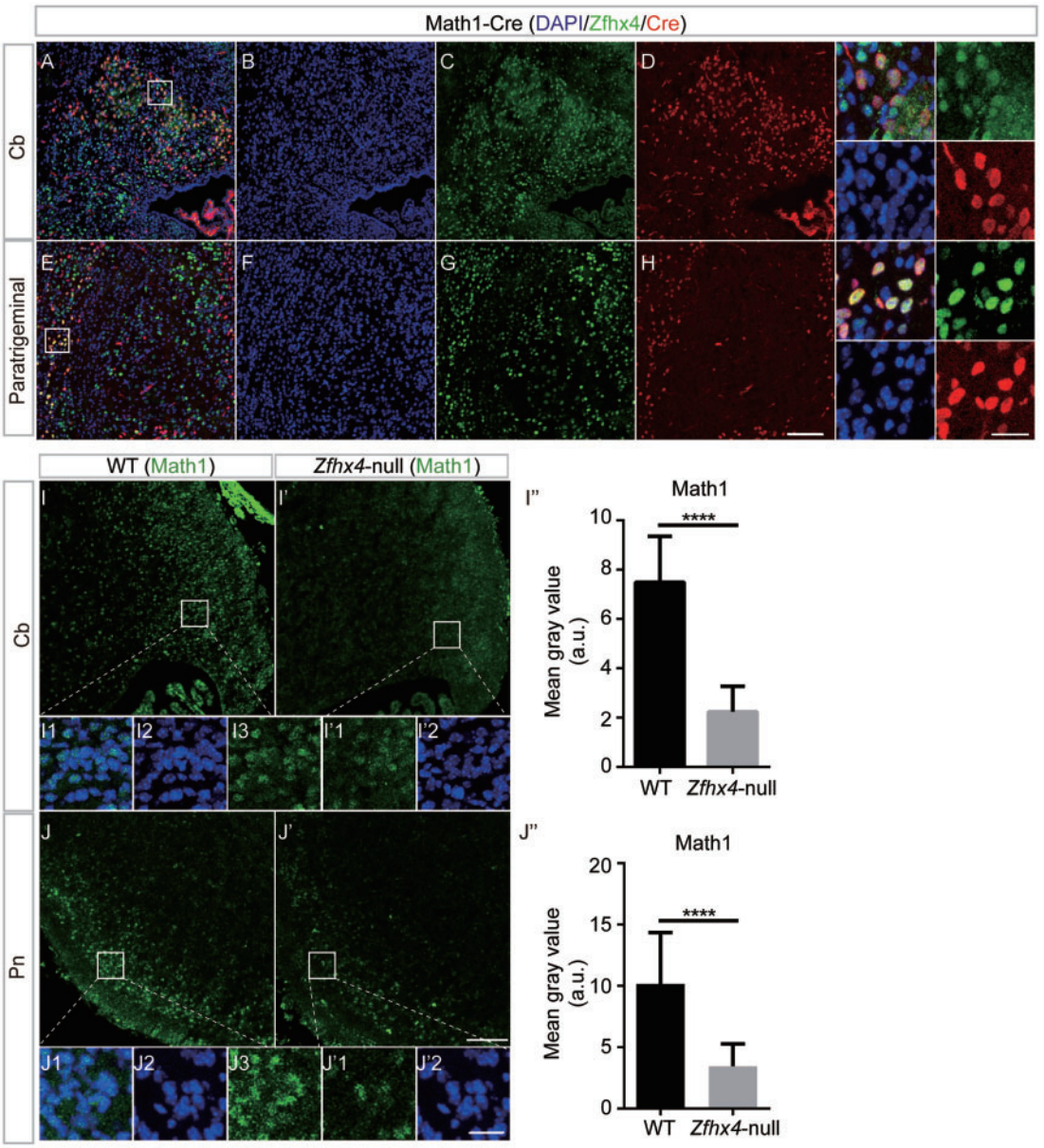

Figure 6 Math1 is coexpressed with Zfhx4 and its expression levels are decreased in *Zfhx4*-null mouse hindbrains. (**A**–**H**) In P0 Math-Cre mice, neurons expressing Math1 were monitored by immunofluorescent staining of Cre. Codistribution of Zfhx4 with Cre in the cerebellum (Cb, **A**–**D**) and paratrigeminal region (**E**–**H**) of P0 Math-Cre mice. DAPI was used to stain nuclei. Insets are magnified neurons showing Zfhx4 (green), Cre (red), and coexpression of Zfhx4 with Math1 (selected regions indicated by solid white rectangles). (**I**–**J"**) Immunofluorescent staining and quantification for Math1 (green) in the Cb and pon (Pn) from P0 WT and *Zfhx4*-null mice. Insets are magnified views of the selected regions indicated by solid white rectangles. Math1 expression decreased in both Cb and Pn of P0 *Zfhx4*-null mice. Scale bar, 100 μm and 25 μm (insets). Data in bar graphs are expressed as mean ± SD. ****$P < 0.0001$ (Student's *t*-test), $n = 15$.

mediate regulatory inputs in response to peripheral or central stimuli. Different neuronal populations of the respiratory network have specific developmental programs and gene expression profiles that are regulated by a set of transcription factors that are specific to particular types of neurons (Blanchi and Sieweke, 2005). Here, we found that *Zfhx4*, a zinc finger homeodomain transcription factor, was highly expressed in the mouse hindbrain, especially in the PRG, VRG, and DRG. Insertion of the *PB* transposon in the third intron led to the ablation of *Zfhx4* gene expression at both mRNA and protein levels. *Zfhx4*-deficient mice died within 24 h after birth and did not show obvious defects in the hearts or lungs. Brain edema

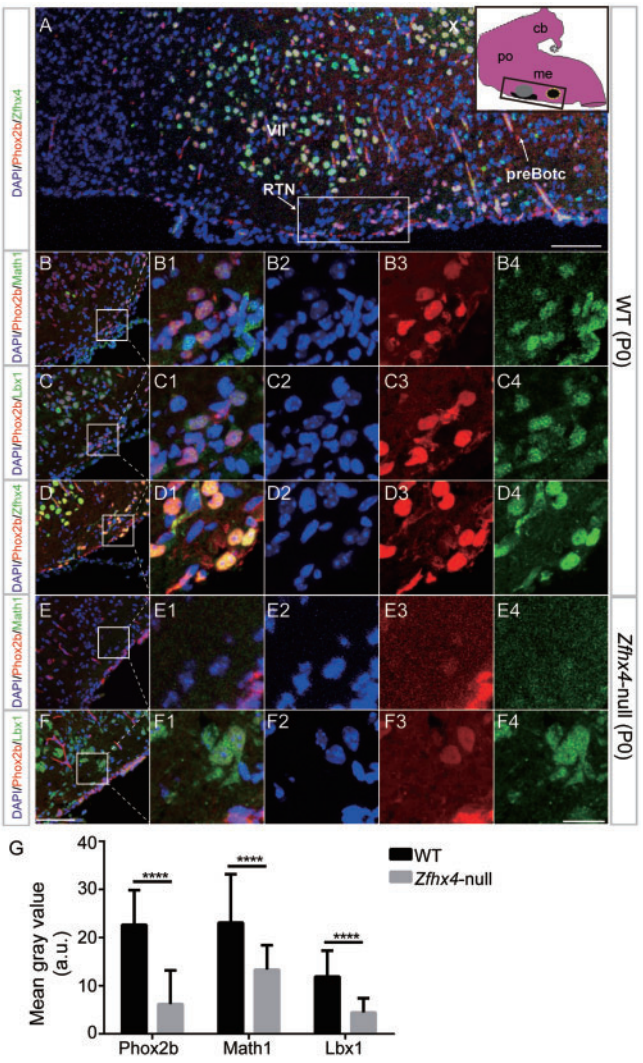

Figure 7 Zfhx4-positive neurons contribute to the development of the RTN. (**A**) Magnification of the ventral respiratory column from P0 WT mouse hindbrain, as indicated by the black rectangle in the inset model of the hindbrain (black ventral region is the RTN, while yellow circle indicates preBotc), showing the coexpression of Phox2b (red) and Zfhx4 (green) in VII and RTN neurons. DAPI was used to stain nuclei. (**B**–**G**) Immunofluorescent staining and quantification for Phox2b, Math1, and Lbx1 in RTN neurons of P0 WT and *Zfhx4*-null mice. RTN region was double-labelled by Phox2b (red) and Math1 or Lbx1 (green) in P0 WT (showing coexpression of Zfhx4 with Phox2b) and *Zfhx4*-null mouse medulla. DAPI was used to stain nuclei. Further magnified images for the selected regions indicated by solid white rectangles are shown to the right. The expression of Phox2b, Math1, and Lbx1 was reduced in the RTN neurons of the P0 *Zfhx4*-null mice. Scale bar, 100 μm and 25 μm (further magnified images). Data in bar graph are expressed as mean ± SD. ****$P < 0.0001$ (Student's *t*-test), $n = 15$.

was observed in the brains of dying mice, but this phenotype was not observed in the embryonic stage or immediately after delivery and might present the phenotype that occurs before death (Supplementary Figure S5). Newborn *Zfhx4*-null mice exhibited gasping behavior and cyanosis. The rhythm of *in vitro* brainstem–spinal cord preparations from *Zfhx4*-null mice was significantly decreased compared with that from WT mice. The above results indicate that this deficit resulted from the disruption of the respiratory center in the hindbrain.

The Zfhx4 protein is highly expressed in several specific areas of the mouse brainstem. To explore the molecular function and mechanism of *Zfhx4* in brainstem respiratory compartments, microarrays were used to detect changes in gene expression in the brainstems of *Zfhx4*-null mice. Several respiratory center development-associated genes were identified to be significantly decreased in *Zfhx4*-null mice compared with WT mice, including *Phox2b* (Dubreuil et al., 2008; Goridis et al., 2010), *Math1* (Machold and Fishell, 2009; Rose et al., 2009), *Lbx1* (Pagliardini et al., 2008), homeobox A2 (*HoxA2*) (Chatonnet et al., 2007), and PC12 ETS domain-containing transcription factor 1 (*Pet-1*) (St-John et al., 2009; Cummings et al., 2010). *Phox2b*, *Math1*, and *Lbx1* attracted our attention, because *Phox2b*, *Math1*, and *Lbx1* knockout mice die at birth and show decreased respiratory frequency and also because these genes are implicated in the development of RTN neurons (Dubreuil et al., 2008; Pagliardini et al., 2008; Machold and Fishell, 2009; Rose et al., 2009; Goridis et al., 2010).

ChIP–seq analysis of brainstem tissues was carried out to identify the direct downstream target genes of Zfhx4. Combined ChIP–seq and mRNA expression microarray analysis revealed that Zfhx4 bound the downstream DNA segment proximal to the transcription start site of the *Phox2b* gene, and this binding was validated by using ChIP–qPCR. This finding indicates that *Phox2b* was the direct downstream target gene of Zfhx4. Immunofluorescence staining revealed that Phox2b was widely coexpressed with Zfhx4 in the P0 brainstem and Phox2b expression was greatly decreased and even undetectable in *Zfhx4*-null mice. Phox2b is a crucial transcription factor for the formation of the RTN of the VRG (Dubreuil et al., 2009; Wang et al., 2013; Pisanski and Pagliardini, 2019). Zfhx4 was expressed in RTN neurons, and ablation of *Zfhx4* led to a significant decrease in the numbers of Phox2b-positive, Math1-positive, and Lbx1-positive neurons. The RTN contains a population of CO_2/H^+-sensitive neurons and functions as the main chemoreceptor (Dubreuil et al., 2009; Wenker et al., 2012; Wang et al., 2013; Fu et al., 2017; Cleary et al., 2020). Our results also showed that the respiration output of *in vitro* brainstem–spinal cord preparations from *Zfhx4*-null mice failed to increase the response to acidification, which indicates that Zfhx4 is involved in and necessary for the proper establishment of the RTN and the reduction in respiratory frequency in *Zfhx4*-null mice may be mainly due to the defective regulatory input of RTN. Furthermore, in the dorsal medulla, the NTS is also Phox2b-dependent and essential for sensory afferents conveying respiratory-related information from the lungs and peripheral chemoreceptors (Dauger et al., 2003; Alheid and McCrimmon, 2008; Zoccal et al., 2014; Fu et al., 2017). Phox2b-expressing LC neurons contribute to the control of breathing most likely via an LC–preBotc circuit (Liu et al., 2021). Our results showed that

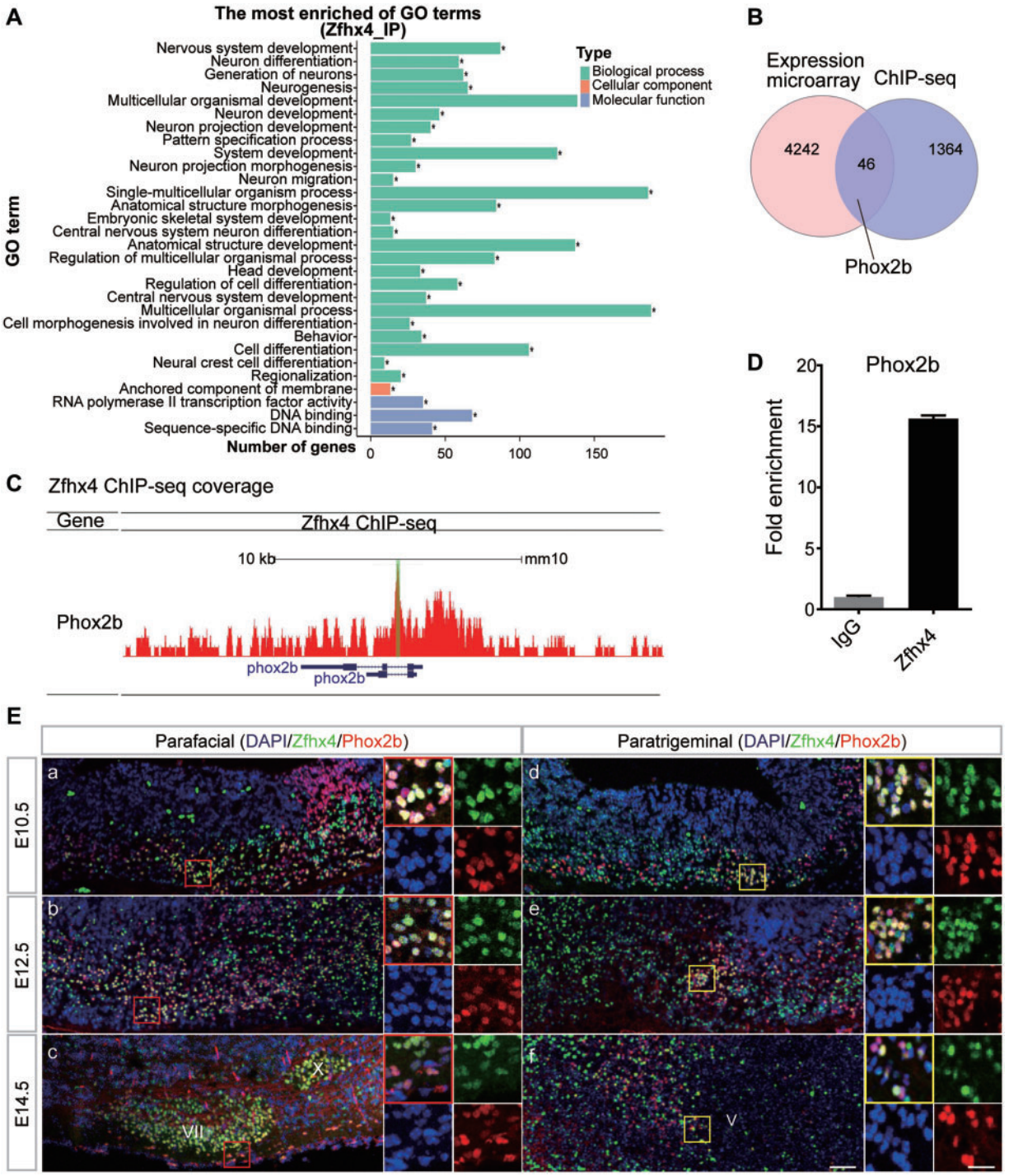

Figure 8 *Phox2b* is the direct downstream target gene of Zfhx4. (**A**) Anti-Zfhx4 ChIP–seq was carried out using E16.5 mouse brainstems and GO enrichment analysis was performed. GO terms with a corrected $P < 0.05$ were considered to be significantly enriched. (**B**) Integrated analysis of the ChIP–seq data and gene expression microarray results (fold change $\geq$1.5). The Venn diagram demonstrating the overlap of 46 genes, which were differently expressed in *Zfhx4*-null mouse brainstems and bound by Zfhx4 protein. *Phox2b* was one of the overlapped genes. (**C**) ChIP–seq binding profile for Zfhx4 at the *Phox2b* loci. (**D**) Anti-Zfhx4 ChIP was carried out using E16.5 mouse brainstems and the recovered DNA was subjected to qPCR analysis by using primers designed for the bound region. Data were normalized to the levels of bound DNA in control IgG IPs and shown as mean ± SD, $n = 3$. (**E**) Sagittal section of paratrigeminal and parafacial regions from E10.5 to E14.5 WT mouse, labelled by Zfhx4 (green) and Phox2b (red). DAPI was used to stain nucleus. The shown paratrigeminal regions were rotated 90 counterclockwise such that the true ventral surface of the pons is facing down, parallel to the ventral surface of the medulla. Insets shown at the right are magnified views from corresponding red and yellow rectangles. Rostral is to the left in a–c; dorsal is to the left in d–f. Scale bar, 100 μm and 25 μm (insets).

Phox2b was coexpressed with Zfhx4 in the NTS and LC, and Phox2b expression was also greatly decreased in those regions in *Zfhx4*-null mice. Furthermore, deep cerebellar neurons and the external granule layer of the cerebellum are Math1-dependent and play roles in proprioception, and the paratrigeminal region of the pons may not be essential for generation of respiratory rhythm but may mediate jugular ganglia-evoked respiratory reflexes (Rose et al., 2009; Driessen et al., 2015, 2018). Our results also showed that Math1 was colocalized with Zfhx4 in the cerebellum and paratrigeminal region in Math1-Cre mice and Math1 expression was reduced in *Zfhx4*-null mice as well. The above results suggest that Zfhx4 expresses and regulates the expression of Phox2b and Math1 in several areas of the respiratory center, and Zfhx4 deficiency results in abnormal development of the RTN, which may be the main cause of rhythm impairment in *Zfhx4*-null mice.

Brain-mediated breathing disorders in humans are often life threatening. To date, the most common causes for congenital hypoventilation are dominant mutations in PHOX2B (Amiel et al., 2003; Sasaki et al., 2003; Weese-Mayer et al., 2003; Hernandez-Miranda et al., 2018), but our knowledge about the etiologies of many other human central respiratory defects remains limited. In this study, *Zfhx4* was identified as a vital gene in the development of the respiratory center and its ablation led to death in the newborn phase; thus, it will be interesting to identify its coding sequence and its expression pattern in newborns with central respiratory defects. *Zfhx4*-deficient mice may provide a useful tool for developing therapeutic approaches for this kind of birth defect.

Materials and methods

Mice and genotyping

The Institutional Animal Care and Use Committee of Fudan University, China approved all protocols. The H362cR1 *PB* insertion mice were obtained from the Institute of Developmental Biology and Molecular Medicine (IDM) at Fudan University in Shanghai, China (Sun et al., 2008). These mice were generated by inserting the *PB* transposon in reverse orientation into the third intron of the *Zfhx4* gene in mice with the FVB/N background. Math-Cre mice were a generous gift from Professor Yifeng Lin (Children's Hospital, Fudan University) (He et al., 2014). Noon on the day on which the vaginal plug was observed was considered E0.5. The genotype of each mouse was determined by PCR analysis of genomic DNA prepared from tail biopsies. Genotyping PCR was performed by using the *PB* forward primer (5′-CTGAGATGTCCTAAATGCACAGCG-3′) for mutants or the *Zfhx4* forward primer (5′-GGCAGAGACAGGCAGATTTC-3′) for WT and the common *Zfhx4* reverse primer (5′-GGGAAAGTGGATTTCTGCAAC-3′).

RNA extraction and qRT-PCR

Total RNA was extracted from tissues using TRIzol reagent (Thermo Fisher) according to the manufacturer's protocol. RNA degradation and contamination were assessed on 1% agarose gels, and the RNA concentration was measured by using a NanoDrop 1000 spectrophotometer (Thermo Scientific). cDNA was synthesized by using the PrimeScript RT reagent Kit with gDNA Eraser (Perfect Real Time; TaKaRa), and the integrity of the synthesized cDNA was confirmed by using glyceraldehyde 3-phosphate dehydrogenase (Gapdh) as the endogenous control. Real-time PCR was carried out using SYBR Premix Ex TaqTM II (Perfect Real Time) (TaKaRa) and measured by using an ABI 7500 instrument. The primers are listed in Supplementary Table S3. PCR was performed as reported by Zhang et al. (2019).

Generation of the anti-Zfhx4 antibody

Specific antiserum against Zfhx4 was raised by using a recombinant mouse Zfhx4 peptide fused to the GST protein. A mouse *Zfhx4* cDNA fragment corresponding to amino acid residues 2677–2884 was generated by PCR from mouse cDNA using mZfhx4-F(BamHI)/mZfhx4-R(NotI) primers and subcloned between the *Bam*HI and *Not*I sites of the PGEX-4T-2 vector (GE Healthcare Life Sciences), and its expression was induced to express by 1 mM isopropyl-β-D-thiogalactoside at 16°C for 5 h hosted by *E. coli* BL21. The GST-Zfhx4 fusion protein was purified by the GST Fusion Protein Purification Kit (Genscript) according to the manufacture's protocol. An immunizing emulsion was prepared by mixing the purified peptide (1 mg/ml in phosphate-buffered saline, pH 7.5) with an equal volume of complete or incomplete Freund's adjuvant. Two rabbits were subcutaneously injected at 10 sites on the back with a total of 2 ml emulsion of 1 mg GST-Zfhx4 and complete Freund's adjuvant (Sigma-Aldrich) on Day 0. Half of the antigens were dissolved in incomplete Freund's adjuvant (Sigma-Aldrich) and used for boost immunization on Days 21, 35, and 49 after the initial immunization. The rabbits were bled on Day 52 to separate the serum. Then, 2 mg GST-Zfhx4 fusion protein was coupled to CNBr-Actived Agarose (Sangon Biotech) according to the manufacture's protocol, and antibodies were purified from the serum with coupled agarose. Anti-GST antibodies were further removed by incubation with 2 mg GST recombinant protein coupled with agarose.

H&E staining

Tissues were immersion fixed with 10% neutral-buffered formalin and embedded in paraffin blocks, and 5 μm sections were prepared on Superfrost Plus slides. The brains were cut sagittally. Sections of the different tissues were stained with hematoxylin and eosin, as reported previously (Xiao et al., 2016; Du et al., 2019).

Immunofluorescence staining

For immunolabelling, the brains of WT and *Zfhx4*-null mouse embryos and neonates were collected at several stages (E10.5–P10). The brains were fixed in 4% PFA at 4°C for 4–10 h and dehydrated with 20% and 30% sucrose for

12 h each. Frozen sections were cut at 10 μm and antibody incubation was performed as previously described (Bermingham et al., 1999). The antibodies and dilutions used in this study were as follows: Zfhx4 (1:2000), Phox2b (1:150, Santa Cruz), Math1 (1:800, Genetex), NeuN (1:500, Temecula), Lbx1 (1:800, Novus), Cre (1:500, Millipore), GFAP (1:1000, Millipore), Alexa Fluor 488-conjugated AffiniPure goat anti-mouse or anti-rabbit IgG, Alexa Fluor 594-conjugated AffiniPure goat anti-mouse or anti-rabbit IgG (1:200, YEASEN), AffiniPure goat anti-chicken IgY (IgG) (H + L) (1:500, Jackson ImmunoResearch), and DAPI nuclear counterstain (1:1000, YEASEN). Primary antibody incubation was performed for 12 h at 4°C and was followed by secondary antibody incubation for 1 h at room temperature. Fluorescence staining was examined by confocal microscopy (Leica TCS SP8 system or Nikon AIR-MP system). Image brightness and contrast were normalized using LAS AF Lite software or NIS-Elements Microscope Imaging Software.

Western blotting

Fresh tissues were lysed with lysis buffer (200 mM Tris–HCl, pH 7.5, 1.5 M NaCl, 10 mM EDTA, 10 mM EGTA, 25 mM sodium pyrophosphate, 10 mM β-glycerophosphate, 1 mM Na_3VO_4, and 50 mM NaF) containing a protease inhibitor cocktail (Roche Diagnostics). The protein lysates were quantified with the Pierce™ BCA Protein Assay Kit (Thermo Fisher). After SDS–PAGE resolution and membrane transfer, the target proteins were probed with primary antibody against Zfhx4 (1:1000) or β-tubulin (1:5000, Proteintech) and then incubated with HRP-conjugated secondary antibodies. Finally, the bands were visualized using a luminescent image analyzer (ImageQuant LAS 4000 mini, GE Healthcare Life Sciences).

In vitro brainstem–spinal cord preparations and electrophysiological experiments

The mice (P0) were deeply anaesthetized with ice. The hindbrain of each animal was exposed, isolated, and immersed in artificial cerebral spinal fluid (ACSF) containing (in mM) 120 NaCl, 8.0 KCl, 1.226 $CaCl_2$, 1.5 $MgCl_2$, 21 $NaHCO_3$, 0.58 NaH_2PO_4, and 30 D-glucose. The solution was constantly bubbled with 95% O_2–5% CO_2 and had a pH of 7.4. The pH of the ACSF was decreased to 7.2 by decreasing the $NaHCO_3$ concentration to 10.5 mM and adjusting the NaCl concentration to 130.5 mM (Dubreuil et al., 2009). The brainstem–spinal cords were dissected under a dissection microscope, and then transferred to the recording chamber and superfused with ACSF (perfusion rate, 5 ml/min) maintained at 25°C ± 1°C.

Recordings from the cervical (C4) ventral roots were made with suction electrodes. The signals were amplified, rectified, low-pass filtered, recorded on computer using an Axopatch 700B amplifier (sampling frequency, 10 kHz; filter frequency, 1 kHz), digitized with 1322A Digidata, and collected and analyzed with Clampex 9.2 software (Axon Instruments). The respiratory frequency was obtained as the frequency of the C4 burst.

Expression microarray

For microarray analysis, a mouse (V2) Gene Expression Microarray 8×60K chip (Agilent) was employed, and the analysis was conducted by CapitalBio Corp. according to the manufacturer's protocols. Briefly, 1 μg of total RNA extracted from the samples was transcribed into double-stranded cDNA by using CbcScript reverse transcriptase and T7-random primers according to the manufacturer's protocol (CapitalBio). The double-stranded cDNA products were purified and *in vitro* transcribed into cRNA with T7 RNA polymerase. After reverse transcription, the cRNA was transcribed into cDNA and labelled with Cy3 by using the Klenow enzyme-labelling strategy, and microarray slides were hybridized with Cy3-labelled probes. Feature Extraction Software v10.7 was used for data extraction from raw microarray image files. Quantile normalization and subsequent data processing were performed using the GeneSpring GX V13.0 software package (Agilent Technologies) (Zhang et al., 2019).

ChIP

ChIP assays were performed by using the Simple ChIP Kit (Cell Signaling Technology, 9005S) with the following adjustments to the standard protocol. Briefly, mouse brainstems were dissected on E16.5, finely minced using a clean scalpel, and then crosslinked with 1.5% formaldehyde. Sonication was performed by using a Bioruptor (Diagenode). The samples were precleared with ChIP-Grade Protein-G magnetic beads and immunoprecipitated by using suitable antibodies: 2 μg IgG (Cell Signaling Technology) and 2 μg Zfhx4. The beads were extensively washed before reverse crosslinking. DNA was purified using a PCR Purification Kit and subsequently used for sequencing or analysis by qPCR. ChIP–seq was performed by the Novogene Experimental Department in China. Clean data were examined via Skewer software (version 0.1.126) and aligned with the unmasked mouse reference genome (GRCm38) by using BWA-men v0.7.12. Peak calling was completed by the model-based analysis of ChIP–seq (MACS) software MACS2 with the default parameters. Replicates of the ChIP–seq data were pooled for downstream analysis.

Statistical analysis

The frequency of the integrated discharges at the C4 root was calculated every minute over a 3-min period. the experiments were repeated under standardized conditions using different preparations obtained from at least three different mice. Quantitation of immunofluorescence ($n = 3$ animals per group) was performed by measuring the mean gray values inside the

regions of interest (ROIs) using ImageJ version 1.48v. At least five measurements were performed for each indicated region on independent sagittal sections. All values in the bar graphs are given as mean ± SD. Statistical analysis was performed using Student's *t*-test or one-way analysis of variance as indicated in the figure legends. The results were considered to be significant when $P < 0.05$. All statistical tests were performed using Prism software (GraphPad, version 6.0).

Acknowledgements

The authors would like to thank Professor Yalin Huang (Fudan University) for her support of immunofluorescence images and Professor Jijiang Wang (Fudan University) for his support of electrophysiological experiments.

Funding

This work was supported by grants from the National Key Research and Development Program of China (2016YFC1000503) and the National Natural Science Foundation of China (81571472, 81741085, and 81971197).

Conflict of interest: none declared.

References

Alheid, G.F., and McCrimmon, D.R. (2008). The chemical neuroanatomy of breathing. Respir. Physiol. Neurobiol. *164*, 3–11.

Amiel, J., Laudier, B., Attie-Bitach, T., et al. (2003). Polyalanine expansion and frameshift mutations of the paired-like homeobox gene PHOX2B in congenital central hypoventilation syndrome. Nat. Genet. *33*, 459–461.

Ben-Arie, N., Bellen, H.J., Armstrong, D.L., et al. (1997). Math1 is essential for genesis of cerebellar granule neurons. Nature *390*, 169–172.

Bermingham, N.A., Hassan, B.A., Price, S.D., et al. (1999). Math1: an essential gene for the generation of inner ear hair cells. Science *284*, 1837–1841.

Blanchi, B., Kelly, L.M., Viemari, J.C., et al. (2003). MafB deficiency causes defective respiratory rhythmogenesis and fatal central apnea at birth. Nat. Neurosci. *6*, 1091–1100.

Blanchi, B., and Sieweke, M.H. (2005). Mutations of brainstem transcription factors and central respiratory disorders. Trends Mol. Med. *11*, 23–30.

Calton, M.A., Howard, J.R., Harper, R.M., et al. (2016). The cerebellum and SIDS: disordered breathing in a mouse model of developmental cerebellar purkinje cell loss during recovery from hypercarbia. Front. Neurol. *7*, 78.

Campbell, R.E., Tour, O., Palmer, A.E., et al. (2002). A monomeric red fluorescent protein. Proc. Natl Acad. Sci. USA *99*, 7877–7882.

Caravagna, C., Kinkead, R., and Soliz, J. (2014). Post-natal hypoxic activity of the central respiratory command is improved in transgenic mice overexpressing Epo in the brain. Respir. Physiol. Neurobiol. *200*, 64–71.

Champagnat, J., Morin-Surun, M.P., Bouvier, J., et al. (2011). Prenatal development of central rhythm generation. Respir. Physiol. Neurobiol. *178*, 146–155.

Chatonnet, F., Wrobel, L.J., Mezieres, V., et al. (2007). Distinct roles of Hoxa2 and Krox20 in the development of rhythmic neural networks controlling inspiratory depth, respiratory frequency, and jaw opening. Neural Dev. *2*, 19.

Chudnovsky, Y., Kim, D., Zheng, S., et al. (2014). ZFHX4 interacts with the NuRD core member CHD4 and regulates the glioblastoma tumor-initiating cell state. Cell Rep. *6*, 313–324.

Cleary, C.M., Moreira, T.S., Takakura, A.C., et al. (2020). Vascular control of the CO_2/H^+ dependent drive to breathe. eLife *9*, e59499.

Cummings, K.J., Li, A., Deneris, E.S., et al. (2010). Bradycardia in serotonin-deficient Pet-$1^{-/-}$ mice: influence of respiratory dysfunction and hyperthermia over the first 2 postnatal weeks. Am. J. Physiol. Regul. Integr. Comp. Physiol. *298*, R1333–R1342.

Czeisler, C.M., Silva, T.M., Fair, S.R., et al. (2019). The role of PHOX2B-derived astrocytes in chemosensory control of breathing and sleep homeostasis. J. Physiol. *597*, 2225–2251.

Dauger, S., Pattyn, A., Frédéric Lofaso, C.G., et al. (2003). Phox2b controls the development of peripheral chemoreceptors and afferent visceral pathways. Development *130*, 6635–6642.

Ding, S., Wu, X., Li, G., et al. (2005). Efficient transposition of the piggyBac (PB) transposon in mammalian cells and mice. Cell *122*, 473–483.

Driessen, A.K., Farrell, M.J., Dutschmann, M., et al. (2018). Reflex regulation of breathing by the paratrigeminal nucleus via multiple bulbar circuits. Brain Struct. Funct. *223*, 4005–4022.

Driessen, A.K., Farrell, M.J., Mazzone, S.B., et al. (2015). The role of the paratrigeminal nucleus in vagal afferent evoked respiratory reflexes: a neuroanatomical and functional study in guinea pigs. Front. Physiol. *6*, 378.

Du, S., Ou, H., Cui, R., et al. (2019). Delivery of Gba gene using AAV9 vector therapy as a treatment strategy in mouse models of gaucher disease. Hum. Gene Ther. *30*, 155–167.

Dubreuil, V., Ramanantsoa, N., Trochet, D., et al. (2008). A human mutation in Phox2b causes lack of CO_2 chemosensitivity, fatal central apnea, and specific loss of parafacial neurons. Proc. Natl Acad. Sci. USA *105*, 1067–1072.

Dubreuil, V., Thoby-Brisson, M., Rallu, M., et al. (2009). Defective respiratory rhythmogenesis and loss of central chemosensitivity in Phox2b mutants targeting retrotrapezoid nucleus neurons. J. Neurosci. *29*, 14836–14846.

Feldman, J.L., Del Negro, C.A., and Gray, P.A. (2013). Understanding the rhythm of breathing: so near, yet so far. Annu. Rev. Physiol. *75*, 423–452.

Friedrich, M.J., Bronner, I.F., Liu, P., et al. (2019). PiggyBac transposon-based insertional mutagenesis in mice. Methods Mol. Biol. *1907*, 171–183.

Fu, C., Xue, J., Wang, R., et al. (2017). Chemosensitive Phox2b-expressing neurons are crucial for hypercapnic ventilatory response in the nucleus tractus solitarius. J. Physiol. *595*, 4973–4989.

Goridis, C., Dubreuil, V., Thoby-Brisson, M., et al. (2010). Phox2b, congenital central hypoventilation syndrome and the control of respiration. Semin. Cell Dev. Biol. *21*, 814–822.

He, X., Zhang, L., Chen, Y., et al. (2014). The G protein α subunit Gαs is a tumor suppressor in Sonic hedgehog-driven medulloblastoma. Nat. Med. *20*, 1035–1042.

Hemmi, K., Ma, D., Miura, Y., et al. (2006). A homeodomain-zinc finger protein, ZFHX4, is expressed in neuronal differentiation manner and suppressed in muscle differentiation manner. Biol. Pharm. Bull. *29*, 1830–1835.

Hernandez-Miranda, L.R., Ibrahim, D.M., Ruffault, P.L., et al. (2018). Mutation in LBX1/Lbx1 precludes transcription factor cooperativity and causes congenital hypoventilation in humans and mice. Proc. Natl Acad. Sci. USA *115*, 13021–13026.

Hernandez-Miranda, L.R., Muller, T., and Birchmeier, C. (2017). The dorsal spinal cord and hindbrain: from developmental mechanisms to functional circuits. Dev. Biol. *432*, 34–42.

Keiko, I., Kiyoshi, K., Hiroshi, O., et al. (2016). The respiratory control mechanisms in the brainstem and spinal cord: integrative views of the neuroanatomy and neurophysiology. J. Physiol. Sci. *67*, 45–62.

Kostich, W.A., and Sanes, J.R. (1995). Expression of zfh-4, a new member of the zinc finger-homeodomain family, in developing brain and muscle. Dev. Dyn. *202*, 145–152.

Li, L., Liu, P., Sun, L., et al. (2016). PiggyBac transposon-based polyadenylation-signal trap for genome-wide mutagenesis in mice. Sci. Rep. *6*, 27788.

Lieske, S.P., Thoby-Brisson, M., Telgkamp, P., et al. (2000). Reconfiguration of the neural network controlling multiple breathing patterns: eupnea, sighs and gasps. Nat. Neurosci. *3*, 600–607.

Liu, N., Fu, C., Yu, H., et al. (2021). Respiratory control by Phox2b-expressing neurons in a locus coeruleus–preBotzinger complex circuit. Neurosci. Bull. *37*, 31–44.

Machold, R.P., and Fishell, G. (2009). Math1: waiting to inhale. Neuron *64*, 293–295.

McMullan, T.W., Crolla, J.A., Gregory, S.G., et al. (2002). A candidate gene for congenital bilateral isolated ptosis identified by molecular analysis of a de novo balanced translocation. Hum. Genet. *110*, 244–250.

Nakashima, M., Nakano, M., Hirano, A., et al. (2008). Genome-wide linkage analysis and mutation analysis of hereditary congenital blepharoptosis in a Japanese family. J. Hum. Genet. *53*, 34–41.

Okada, Y., Kawai, A., Mückenhoff, K., et al. (1998). Role of the pons in hypoxic respiratory depression in the neonatal rat. Respir. Physiol. *111*, 55–63.

Onimaru, H., and Homma, I. (2003). A novel functional neuron group for respiratory rhythm generation in the ventral medulla. J. Neurosci. *23*, 1478–1486.

Onimaru, H., Ikeda, K., and Kawakami, K. (2012). Postsynaptic mechanisms of CO_2 responses in parafacial respiratory neurons of newborn rats. J. Physiol. *590*, 1615–1624.

Pagliardini, S., Ren, J., Gray, P.A., et al. (2008). Central respiratory rhythmogenesis is abnormal in lbx1-deficient mice. J. Neurosci. *28*, 11030–11041.

Palomares, M., Delicado, A., Mansilla, E., et al. (2011). Characterization of a 8q21.11 microdeletion syndrome associated with intellectual disability and a recognizable phenotype. Am. J. Hum. Genet. *89*, 295–301.

Pisanski, A., and Pagliardini, S. (2019). The parafacial respiratory group and the control of active expiration. Respir. Physiol. Neurobiol. *265*, 153–160.

Porzionato, A., Macchi, V., and De Caro, R. (2018). Central and peripheral chemoreceptors in sudden infant death syndrome. J. Physiol. *596*, 3007–3019.

Ramanantsoa, N., and Gallego, J. (2013). Congenital central hypoventilation syndrome. Respir. Physiol. Neurobiol. *189*, 272–279.

Ray, R.S., Corcoran, A.E., Brust, R.D., et al. (2013). Egr2-neurons control the adult respiratory response to hypercapnia. Brain Res. *1511*, 115–125.

Rose, M.F., Ren, J., Ahmad, K.A., et al. (2009). Math1 is essential for the development of hindbrain neurons critical for perinatal breathing. Neuron *64*, 341–354.

Ruffault, P.L., D'Autreaux, F., Hayes, J.A., et al. (2015). The retrotrapezoid nucleus neurons expressing Atoh1 and Phox2b are essential for the respiratory response to CO_2. eLife *4*, e07051.

Sakata, N., Hemmi, K., Kawaguchi, M., et al. (2000). The mouse ZFH-4 protein contains four homeodomains and twenty-two zinc fingers. Biochem. Biophys. Res. Commun. *273*, 686–693.

Sasaki, A., Kanai, M., Kijima, K., et al. (2003). Molecular analysis of congenital central hypoventilation syndrome. Hum. Genet. *114*, 22–26.

St-John, W.M., Li, A., and Leiter, J.C. (2009). Genesis of gasping is independent of levels of serotonin in the Pet-1 knockout mouse. J. Appl. Physiol. *107*, 679–685.

Sun, L.V., Jin, K., Liu, Y., et al. (2008). PBmice: an integrated database system of piggyBac (PB) insertional mutations and their characterizations in mice. Nucleic Acids Res. *36*, D729–D734.

Thoby-Brisson, M., Karlen, M., Wu, N., et al. (2009). Genetic identification of an embryonic parafacial oscillator coupling to the preBotzinger complex. Nat. Neurosci. *12*, 1028–1035.

Trochet, D., O'Brien, L.M., Gozal, D., et al. (2005). PHOX2B genotype allows for prediction of tumor risk in congenital central hypoventilation syndrome. Am. J. Hum. Genet. *76*, 421–426.

Wang, S., Shi, Y., Shu, S., et al. (2013). Phox2b-expressing retrotrapezoid neurons are intrinsically responsive to H^+ and CO_2. J. Neurosci. *33*, 7756–7761.

Weber, J., de la Rosa, J., Grove, C.S., et al. (2019). PiggyBac transposon tools for recessive screening identify B-cell lymphoma drivers in mice. Nat. Commun. *10*, 1415.

Weese-Mayer, D.E., Berry-Kravis, E.M., Zhou, L., et al. (2003). Idiopathic congenital central hypoventilation syndrome: analysis of genes pertinent to early autonomic nervous system embryologic development and identification of mutations in PHOX2b. Am. J. Med. Genet. A *123A*, 267–278.

Weese-Mayer, D.E., Rand, C.M., Zhou, A., et al. (2017). Congenital central hypoventilation syndrome: a bedside-to-bench success story for advancing early diagnosis and treatment and improved survival and quality of life. Pediatr. Res. *81*, 192–201.

Wenker, I.C., Sobrinho, C.R., Takakura, A.C., et al. (2012). Regulation of ventral surface CO_2/H^+-sensitive neurons by purinergic signalling. J. Physiol. *590*, 2137–2150.

Wuyam, B., Pepin, J.L., Tremel, F., et al. (2000). Pathophysiology of central sleep apnea syndrome. Sleep *23(Suppl. 4)*, S213–S219.

Xiao, J., Jin, K., Wang, J., et al. (2016). Conditional knockout of TFPI-1 in VSMCs of mice accelerates atherosclerosis by enhancing AMOT/YAP pathway. Int. J. Cardiol. *228*, 605.

Yap, W.S., and Fleetham, J.A. (2001). Central sleep apnea and hypoventilation syndrome. Curr. Treat. Opt. Neurol. *3*, 51–56.

Zhang, M., Jiang, N., Cui, R., et al. (2019). Deregulated lncRNA expression profile in the mouse lung adenocarcinomas with KRAS-G12D mutation and P53 knockout. J. Cell. Mol. Med. *23*, 6978–6988.

Zoccal, D.B., Furuya, W.I., Bassi, M., et al. (2014). The nucleus of the solitary tract and the coordination of respiratory and sympathetic activities. Front. Physiol. *5*, 238.

Zoccal, D.B., Silva, J.N., Barnett, W.H., et al. (2018). Interaction between the retrotrapezoid nucleus and the parafacial respiratory group to regulate active expiration and sympathetic activity in rats. Am. J. Physiol. Lung Cell. Mol. Physiol. *315*, L891–L909.